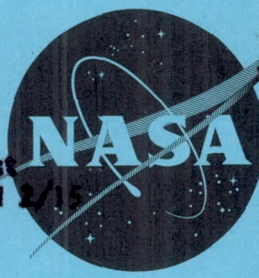62 71938

Copy

35

NASA TM X-114

NASA TM X-114

Classification changed to declassifie
effective 1 April 1963 under
authority of NASA CCN 2 by
J. J. Carroll.

AUTHORITY
1. AF600 416-0 1 2   3j
2. Memo 0 ... R5   ... Subject
 ... Cttg Dtd 2/15

N63 - 13893

Code-1

TECHNICAL MEMORANDUM
X-114

AN EXPERIMENTAL INVESTIGATION IN AN ATMOSPHERE

ENTRY SIMULATOR OF NYLON AS AN ABLATIVE

MATERIAL FOR BALLISTIC MISSILES

By Gary H. Bowman and Raymond C. Savin

Ames Research Center
Moffett Field, Calif.

OTS PRICE

XEROX $

MICROFILM $

553983 38p

CLASSIFIED DOCUMENT - TITLE UNCLASSIFIED

NATIONAL AERONAUTICS AND SPACE ADMINISTRATION

WASHINGTON   December 1959

NATIONAL AERONAUTICS AND SPACE ADMINISTRATION

TECHNICAL MEMORANDUM X-114

AN EXPERIMENTAL INVESTIGATION IN AN ATMOSPHERE

ENTRY SIMULATOR OF NYLON AS AN ABLATIVE

MATERIAL FOR BALLISTIC MISSILES*

By Gary H. Bowman and Raymond C. Savin

SUMMARY

Tests were conducted in a small-scale atmosphere-entry simulator to investigate the feasibility of nylon as an ablative material for long-range ballistic missiles. The test models were spherically tipped cone cylinders 0.22 inch in diameter. The cone half-angles varied from 40° to 90° and the tip radius was equal to approximately one fourth of the model diameter. The tests simulated the motion and heating associated with the atmosphere entry of ballistic missiles having entrance velocities ranging from 13,300 to 19,800 feet per second, diameters from 2.6 to 2.9 feet, weights from 707 to 930 pounds, and maximum ranges from 1218 to 3400 statute miles, respectively.

Studies of models recovered after flight through the simulator indicate that nylon is capable of withstanding the thermal stresses associated with atmosphere-entry heating. These studies also indicate that increasing cone angle causes, for the most part, a slight decrease in ablation; whereas, increasing entry velocity causes an increase in ablation. The weight loss due to ablation is about 2 percent or less of the initial model weight in all cases tested, which indicates that nylon is an effective ablative material for long-range ballistic missiles.

INTRODUCTION

The aerodynamic heating associated with the atmosphere entry of a ballistic missile can impose severe weight penalties on a vehicle since some method of structural cooling must be employed. Currently one of the more promising methods of providing the required cooling is the use of an ablation heat shield. With this method the forward face of a

---

*Title, Unclassified

missile is covered with expendable material which, as it ablates, absorbs heat by essentially utilizing its heat capacity and latent heat of vaporization. In addition, the vapor injection into the air boundary layer may also block a large fraction of heat from reaching the surface.

Recent theoretical and experimental investigations (see, e.g., refs. 1 and 2) have indicated that some materials belonging to the plastics group have attractive ablation characteristics. Unfortunately, the ablation cooling provided by many of these materials (e.g., nylon) is as yet not amenable to accurate theoretical treatment since application of theory depends to such a great extent on a knowledge of unavailable material properties in various states (i.e., solid, liquid, and gaseous). Although there are some experimental data available for nylon and other materials, these data have been obtained, in general, under conditions which do not simulate the history of the heating associated with the atmosphere entry of a full-scale vehicle. As a result, certain important aspects of material capability (e.g., structural ability to withstand thermal stress due to this heating) have in most cases not been determined. Another example would be the net weight loss over the trajectory.

The motion and heating of a ballistic missile during atmosphere entry can be simulated with the small-scale atmosphere-entry simulator at the Ames Research Center. Thus, the simulator is particularly suited for studies in which heating history plays an important role. Accordingly, an exploratory investigation of the effectiveness of nylon as an ablative material for long-range ballistic missiles was conducted with this equipment. The results of this investigation are the subject of this report.

NOTATION

c_p specific heat at constant pressure

c_S specific heat of material up to melting point

C_D drag coefficient referred to base area

D diameter of model or missile

h specific enthalpy

H_L heat capacity of solid-liquid system

k thermal conductivity

l length

L_S latent heat of fusion

L_V latent heat of vaporization

$\dot{m}_L$ mass rate of ablation per unit area

$\dot{m}_V$ mass rate of vaporization per unit area

M molecular weight ratio of air to material vapor

p static pressure

Pr Prandtl number

$\dot{q}$ local heating rate per unit area

$\bar{\dot{q}}$ average heating rate per unit area

Q total convective heat absorbed

Q^* effective heat of ablation per unit mass

$\bar{Q}^*$ average effective heat of ablation per unit mass over trajectory

r nose radius of model or missile

R missile range

Re_∞ free-stream Reynolds number referred to hemispherical nose radius of model

s distance along gas-liquid interface

S nose surface area of model or missile

t time

T temperature

T_m melting temperature

V velocity

$\bar{\dot{w}}$ average rate of ablation weight loss per unit area

W initial weight of model or missile

ΔW weight lost due to ablation

x distance along axis of model or missile

y   distance normal to gas-liquid interface

α thermal diffusivity

δ_c conical half-angle of model or missile

θ inclination of flight path from horizontal

μ viscosity

ρ density

τ shear stress

ψ ratio of heat transfer with and without vaporization

Subscripts

E   entrance conditions for simulated and real atmosphere

i   conditions at gas-liquid interface

L   material property in liquid state

mi   property associated with missile

mo   property associated with model

o   nonablating surface

S   material property in solid state

t   stagnation conditions

V   material property in vapor state

APPARATUS AND TESTS

Test Apparatus

        Tests were conducted in the Ames small-scale atmosphere-entry
simulator. A detailed description of this equipment may be found in
reference 3. In the present tests, the single-stage light-gas gun was
employed to obtain model velocities (relative to the air stream) up to
approximately 16,000 feet per second. To obtain higher velocities

(up to 20,000 feet per second), the gun was modified to include a
second-stage pump tube and, thereby, provide a means of compressing the
driving gas, helium, to higher pressures and temperatures.

Models

The test models were 0.22 caliber and were machined from nylon
(Polypenco 101). They consisted of a spherically tipped conical nose
and a cylindrical afterbody. The cone half-angles employed were 40°,
50°, 60°, 70°, and 90°. The nose radius was held constant and equal to
0.053 inch or approximately one fourth of the afterbody diameter. Since
the forebody dimensions changed with cone angle, the afterbody length
was varied to maintain the same weight of approximately 0.105 gram for
all models. Dimensions of the models are given in figure 1.

Test Procedure

Prior to each test, the model weight and afterbody length and
diameter were measured. All models were launched and a time-distance
history was determined in the manner described in reference 3. Entrance
velocities ranged from approximately 13,300 to 19,800 feet per second
relative to the air stream. The terminal velocity was maintained nearly
constant at approximately 1000 feet per second. The models were recovered
at the end of their flight in soft balsawood catcher material. The
recovered models were then weighed and measured to determine their weight
losses and any changes in dimensions.

Reduction of Data

There are three possible causes of weight loss from a model fired
in simulation: (1) launching, (2) recovery, and (3) flight through the
simulated atmosphere. The latter or ablation weight loss can be deter-
mined only as a result of a careful evaluation of the weight losses due
to launching and recovery and subtraction of these losses from the total
measured weight loss. The weight loss due to launching was determined
from the changes in afterbody length and the decrement in diameter due
to the scraping of the model along the launch tube. The change in length
caused by the hot helium gases scrubbing the base of the model during
launching was found to be negligible. The weight loss due to recovery
of the model was determined by a series of penetration tests. Models of
the same weight and shape were launched at velocities comparable to the
impact velocities of the simulation tests (approximately 1000 feet per
second) and allowed to penetrate soft balsawood blocks - the same type

of material employed as catcher blocks for the tests. These tests indicated a negligible weight loss due to recovery. Accordingly, the weight lost by ablation during atmosphere entry was determined by subtracting the weight loss due to launching from the total weight loss of the test model. In general, the ablation weight loss amounted to about 60 percent of the total weight loss.

Accuracy of Test Results

Errors in determining model weight losses can arise principally from the following two sources: (1) the measurement of the afterbody length and diameter and (2) the weighing of the models. The afterbody length of each model was measured to ±0.0002 inch prior to its flight through the simulator and the diameter was measured to ±0.0002 inch before and after the test. Each model was also weighed to ±0.00005 gram before and after the test. These limits of measurement result in a maximum probable error of approximately ±20 percent of the average minimum ablation weight loss observed.

RESULTS AND DISCUSSION

It has been demonstrated in reference 4 that the total convective heat per unit mass and resulting thermal stresses associated with the atmosphere entry of a ballistic missile can be duplicated with a small-scale test model in an atmosphere-entry simulator. The simulation requires that the model and missile surfaces be geometrically similar and made of the same material and that the velocities and local Reynolds numbers be the same at corresponding points in the trajectory. The degree to which the present test conditions simulate the motion of full-scale ballistic missiles is indicated in figure 2. In this figure, theoretical velocities for a simulated missile along with experimental velocities obtained for the test model are shown as a function of simulated altitude. The simulation of altitude requires the product of ambient density and vehicle diameter (i.e., ρD) to be the same for model and missile. The results shown in this figure are representative of the test results in general. The data points were determined from one time-distance history obtained for the 50° cone half-angle model launched at a velocity (relative to the air stream) of 15,600 feet per second. The dimensions of the simulated missile shown in the figure were determined according to reference 4. The entry angle, θ_E, and corresponding range were determined from the method of reference 5 and the theoretical velocities were calculated according to reference 6. The agreement between the theoretical and experimental velocities indicates that the requirement of equal velocity for model and missile at corresponding points in the trajectories is essentially satisfied. The experimental velocities are somewhat lower

than the theoretical values near the end of the trajectory. However,
the terminal velocities are small in both cases. Since the total heat
absorbed per unit mass is proportional to the difference in the square
of entrance and terminal velocities (see ref. 4), the error in simulat-
ing the total heating per unit mass is negligibly small for our purposes.

The range of the present investigation is indicated in the following
table which lists the characteristics of the missiles whose atmosphere
entry was simulated.

δ_c, deg	V_E, ft/sec	θ_E, deg	Diameter, ft	Weight, lb	Range, statute miles
40	15,600	38	2.7	760	1806
50	↓	↓	↓	↓	↓
60					
70					
90					
50	13,300	41	2.6	707	1218
	17,300	37	2.8	805	2318
	19,800	33	2.9	930	3400

These characteristics were determined in the manner just described.
Thus, for the first group listed, the tests simulated the flight of
missiles having shapes similar to the test models with a diameter of
2.7 feet, a weight of 760 pounds and, according to reference 5, a total
range of 1806 statute miles when entering the earth's atmosphere at 38°
to the horizontal at a velocity of 15,600 feet per second. For an
entrance velocity of 19,800 feet per second, the missile will be slightly
larger, will weigh 930 pounds, and will have a range of 3400 statute
miles.

Let us first consider the results of the tests from the standpoint
of the structural feasibility of nylon as an ablation heat shield for
ballistic missiles. One qualitative measure of this feasibility is
readily obtained from an examination of the test models after their
flight through the simulator. In this connection, the majority of models
recovered showed no evidence of cracking even at test velocities of
19,800 feet per second. Because of the infrequency of cracking, it is
believed that the cracks were caused by the stresses imposed in launching
the models.[1] Aside from the occasional cracking, the models also experi-
enced surface pitting. As indicated by the photographs of the 50° cone
half-angle test models in figure 3, the pitting was more severe at the
higher velocities. Conclusive evidence as to the cause of this pitting

------

[1]The test models experienced accelerations up to approximately
15 million g's during launching. The decelerations experienced by the
models, being of the same order as the accelerations, were also higher
than those associated with a full-scale missile.

is lacking at present. More study is needed to determine whether it was caused by surface spalling or, as noted in reference 3 with copper-faced models, by impurities in the air stream.

It should be mentioned that the solid models employed in the tests, being more rigid, will tend to fail more readily under thermal loading than would a relatively thin shield of the same material on the face of the model. In this connection, the analysis presented in appendix A indicates that the depth to which heat was conducted into the models was much less than 1 percent of the model diameter. This depth (a fraction of an inch for the simulated full-scale missile) is considerably less than might be required for a practical heat shield. Thus, the presence of the additional ablation material in the core of the model did not affect the heat capacity of the models in the tests. It would appear, then, on the basis of these qualitative results, that nylon is an effective heat shield material.

The next point to be considered is the amount of nylon required as an ablation heat-sink material. An indication of the amount of surface material lost due to ablation is shown in figure 4. These photographs were made by projecting the silhouette of recovered models ($\delta_c = 50^\circ$) onto a screen containing a template of the pretest model profile. Since the proper orientation of the template with respect to the recovered models was difficult to achieve, the photographs do not provide an accurate measure of the total amount of material lost. They do indicate, however, that the greatest thickness of material was lost from the spherical segment of the nose. It appears also that ablation has taken place over a greater area of the nose in the case of the model launched at the higher velocity. It is further indicated in this latter case that nose material has been lost in a localized region near the sphere-cone juncture. An ablation distribution of this type might be expected in the presence of transition to turbulent boundary-layer flow, since for this type of flow the heat-transfer rate reaches its maximum value downstream of the stagnation point (see ref. 7). It was not possible to determine the type of boundary layer on the models during flight. However, it may be deduced from the free-stream Reynolds number values shown in figure 5 that turbulent flow might well have existed in the region of the sphere-cone juncture at the higher entrance velocities.

The actual measured weight losses due to ablation of the test models are shown in figures 6 and 7. The variation of percent weight loss with model shape is shown in figure 6. The drag coefficients indicated on the figure were computed from Newtonian theory. Each datum point represents the average weight loss obtained in launching four to five models at an entrance velocity of about 15,600 feet per second. The root-mean-square deviation from the average is also indicated. There are two things to be noted from this figure. First, one may speculate that the minimum weight losses observed indicate that the 60° and 70° models approach shapes having

minimum heat transfer. Perhaps the point of greater importance, however, is that the ablation weight loss appears to be less than 2 percent of the initial model weight for a rather large range of nose shapes. The implication of this result is that one has a rather wide latitude in choice of shape at a cost of a relatively low weight penalty. The effect of entrance velocity on the ablation weight loss is shown in figure 7. These data were obtained as a result of launching 50° cone half-angle models over a range of velocities from 13,300 to 19,800 feet per second as indicated. Again the weight loss is about 2 percent or less over the velocity range. On the basis of these and previously discussed results, nylon appears to be an effective ablation heat shield material.

It is appropriate now to consider the test results in terms of the effective heat capacity of nylon. To this end, consider an effective heat of ablation parameter, Q^{*}, defined as the ratio of heating rate per unit area at the nose of a nonablating body to the rate of weight loss per unit area. Then, in terms of time-averaged quantities,

$$\bar{Q}^{*} = \frac{\bar{\dot{q}}_{o}}{\bar{\dot{w}}}$$

where the average heating rate is simply

$$\bar{\dot{q}}_{o} = \frac{Q}{tS}$$

and Q is the total convective heat transferred to the nose area, S, over the trajectory time, t, and

$$\bar{\dot{w}} = \frac{\Delta W}{tS}$$

where ΔW is the total weight lost due to ablation. Therefore, $\bar{Q}^{*}$ can also be expressed in the form

$$\bar{Q}^{*} = \frac{Q/W}{\Delta W/W}$$

Accordingly, if $\bar{Q}^{*}_{mo} = \bar{Q}^{*}_{mi}$, the fraction of weight lost will be the same in model and missile since the total heat per unit weight is duplicated (ref. 4).

The data for the 50° test models have been reduced to values of $\bar{Q}^{*}$ according to the above relation. The values of Q, the total heat transferred to the model, were calculated for two cases: (1) the flow

downstream of the stagnation point was all laminar and (2) the flow was
all turbulent. The laminar heating rates were calculated in the manner
of reference 8 and the turbulent rates as suggested in reference 7. The
stagnation heat flux was determined according to the analysis of refer-
ence 9. The transient time required for the onset of ablation was neg-
lected since the analysis of appendix A demonstrates this approximation
to be justified. The variation of average effective heats of ablation
for both laminar and turbulent heating rates is shown plotted in figure 8
as a function of the stagnation enthalpy, h_{t_E}, corresponding to the
initial point in the trajectory. Because of the relatively high veloci-
ties under consideration, the relation

$$h_{t_E} \approx \frac{V_E^2}{2}$$

was employed in determining the specific enthalpies. Since the entrance
velocity is the same for model and missile, the stagnation enthalpy is
essentially duplicated.

An analysis of the degree to which simulation of the ablation process
can be achieved in tests of the present type is presented in appendix B.
It is indicated by this analysis that if the ablation process is purely
one of liquefaction then the test results for Q^* are too large and must
be corrected before they can be applied to a full-scale missile; however,
if ablation takes place solely as a result of vaporization, then the test
results are essentially applicable without correction. In order to esti-
mate the correction in the case of liquefaction, it is necessary to know
the thermal properties of the ablating material in its solid and liquid
states. Unfortunately, there appears to be a dearth of information con-
cerning the liquid-state properties, not only for nylon, but for thermo-
plastics in general. Calculations were carried out for pyrex glass for
which the pertinent properties are available. The results are shown in
figure 9, where a maximum correction of about 10 percent in Q^* is indi-
cated for scale factors corresponding to the present tests (i.e.,
$D_{mi}/D_{mo} \approx 150$). It should be noted that nylon has a melting temperature
of about 500° to 600° F. Some data presented in reference 10 indicate
that the vaporization temperature of nylon, or perhaps more properly
depolymerization temperature, is approximately 600° to 700° F in a vacuum.
Although one would expect higher depolymerization temperatures at higher
pressures, it is believed that the surface could not maintain much higher
temperatures without depolymerizing. In this connection, it should be
mentioned that little, if any, evidence of melting could be detected from
recovered test models. It is reasoned on this basis that the depolymeri-
zation temperature is close to the melting temperature and therefore
essentially all the ablation will take place by surface depolymerization
in both model and missile. Thus, for laminar flow, the conclusion of

case (b) in appendix B[2] (i.e., $\dot{m}_V/\dot{m}_L \rightarrow 1$) is applicable to the present test results;[3] namely, $Q^*_{mo} \approx Q^*_{mi}$. In the case of turbulent flow, the situation may not be the same. However, it does not appear illogical to assume comparable simulation (to the laminar flow case) in view of the fact that the local Reynolds numbers and driving enthalpies are essentially duplicated in model and missile.

CONCLUDING REMARKS

Tests have been conducted in the small-scale atmosphere-entry simulator to assess the feasibility of nylon as an ablation heat shield material. The test models consisted of spherically tipped cone cylinders which had a diameter of 0.22 inch and weighed approximately 0.1 gram. The cone half-angle varied from 40° to 90° and the tip radius was equal to approximately one fourth the afterbody diameter. The tests simulated the motion and heating associated with the atmosphere entry of ballistic missiles having entrance velocities ranging from 13,300 to 19,800 feet per second, diameters from 2.6 to 2.9 feet, weights from 707 to 930 pounds, and maximum ranges from 1218 to 3400 statute miles, respectively.

Nylon was found to be a structurally attractive material from the standpoint of withstanding the thermal loading associated with the atmosphere entry of ballistic missiles. Ablation weight loss was found to decrease with increasing cone half-angle up to 60° and remained essentially constant or increased slightly for blunter shapes. Increasing velocity caused an increase in ablation. The measured weight loss due to ablation was about 2 percent or less of the initial model weight in all cases. On the basis of a qualitative simulation analysis also presented, it was indicated that these results are approximately applicable to full-scale ballistic missiles. In view of these findings, it is concluded that nylon is an effective ablation heat shield material for long-range ballistic missiles.

Ames Research Center
    National Aeronautics and Space Administration
        Moffett Field, Calif., Aug. 13, 1959

---

[2]The conclusions of appendix B for the stagnation point can be shown to hold downstream along the body surface by means of Lees' "local similarity" assumptions (ref. 8) which have been, in essence, verified experimentally (ref. 11).

[3]It should be noted from appendix A that the transient time is simulated when $Q^*_{mo} = Q^*_{mi}$.

APPENDIX A

ESTIMATE OF THERMAL THICKNESS AND TRANSIENT

TIME FOR ONSET OF ABLATION

Initial Surface Temperature Rise

The variation of surface temperature with time, t, on a semi-infinite solid may be expressed in the form (see ref. 12)

$$T = \frac{1}{k} \sqrt{\frac{\alpha}{\pi}} \int_0^t \frac{\dot{q}_o(\xi)}{\sqrt{t - \xi}} \, d\xi \tag{A1}$$

where k is the thermal conductivity and α is the thermal diffusivity of the solid. Now the heat-transfer rate, $\dot{q}_o$, is larger in the simulator by the ratio of missile to model diameter (see ref. 4). If we require the surface temperature to be the same in model and missile, then according to equation (A1), t must be smaller in the simulator by the square of the ratio of model to missile diameter. This relation is identical to the simulation requirement for the trajectory times of model and missile obtained in reference 4. Therefore, prior to the onset of ablation, the fraction of trajectory time required for the surface to heat up is duplicated in model and missile.

The variation of surface temperature at the stagnation point with time for the trajectory corresponding to $V_E = 15,600$ feet per second was calculated from equation (A1). The following thermal properties of nylon were employed in these and all subsequent calculations: k = 0.1405 Btu/hr-ft ^{O}F, c_p = 0.40 Btu/lb ^{O}F, ρ = 68.6 lb/cu ft. Since the heat-transfer rate, $\dot{q}_o$, varies with time, the integral was evaluated graphically. The results are presented in figure 10 where it is evident that the surface temperatures become large in a matter of microseconds. If the average heat-transfer rate over the nose had been used to calculate the surface temperatures, the resulting times would be approximately four times those shown. They would still be negligible, however, compared to the test flight time of 1 millisecond.

Thickness of Thermal Layer

Since the initial temperature rise occurs over such a small interval of time, the heating rate can be assumed constant during this period. The relation defining the temperature at each point in a homogeneous semi-infinite solid at time t is then given by (see ref. 12)

$$T = \frac{\dot{q}_O}{k} \left[2\sqrt{\frac{\alpha t}{\pi}}\, e^{-\frac{x^2}{4\alpha t}} - x\ \text{erfc}\left(\frac{x}{2\sqrt{\alpha t}}\right) \right] \tag{A2}$$

It should be noted that relations (A1) and (A2) become identical for
$x = 0$ and $\dot{q}_O$ = constant. The temperature distribution through the model
was calculated from equation (A2) for t corresponding to a surface
temperature of 1000° F (see fig. 10). The stagnation heating rate cor-
responding to the initial point in the trajectory was used in the calcu-
lations; namely, at $V = V_E = 15{,}600$ ft/sec, $(\dot{q}_O)_t = 35{,}000$ Btu/sq ft-sec.
The results are shown in figure 11. For convenience, the initial temper-
ature of the model interior has been taken as 0° F. It is clear from
these results that the heat conduction effects are confined to a region
of thickness approximately 0.02 percent of the model diameter. This
percentage thickness is substantially less than the shell thickness
required to simulate a practical heat shield for a full-scale missile.

Transient Time for Steady-State Ablation

After the surface has reached a temperature sufficiently high for
the onset of ablation, there is a further time lag or transient time for
ablation to attain a state of equilibrium. An order of magnitude esti-
mate of this transient time may be obtained from the relation (see
ref. 13)

$$t = \frac{k_S \rho_S}{c_S} \left(\frac{Q^*}{\dot{q}_O}\right)^2 \tag{A3}$$

It is interesting to note from this expression that if $Q^*_{mo} = Q^*_{mi}$, the
transient time will be smaller for the model by the square of the ratio
of model to missile diameters (note $\dot{q}_O \sim 1/D$ from ref. 4). Therefore,
the fraction of trajectory time required for the transient time will be
the same for model and missile. A typical transient time for the present
tests has been calculated employing an average value of $\dot{q}_O$ and for the
trajectory corresponding to $\delta_c = 90^O$ and $V_E = 15{,}600$ ft/sec; namely,
$\bar{\dot{q}}_O = 12{,}000$ Btu/sq ft-sec and $\bar{Q}^* = 1000$ Btu/lb (see fig. 8). The result-
ing transient time is about 0.05 millisecond which is about 5 percent of
the total flight time.

APPENDIX B

THEORETICAL ESTIMATE OF ABLATION

WEIGHT LOSS SIMULATION

Relatively simplified expressions for steady-state surface ablation phenomena have recently been obtained by Lees (ref. 7) and Bethe and Adams (ref. 14). The purpose of the following analysis is to utilize the results of these studies in an effort to obtain an estimate of the degree to which simulator test results are applicable to full-scale missiles. For details of the development of the basic equations and for the simplifying assumptions involved, the reader is referred to the references cited above. For simplicity, the following analysis is restricted to the stagnation region of a blunt body.

With these points in mind, and on the basis of the analyses of references 7 and 14, the energy, momentum, and continuity equations may be combined to yield

$$\dot{m}_L - \dot{m}_V = \frac{2\rho_L \bar{k}_L{}^2 T_i{}^2 \tau_i{}'}{A^2 c_{p_L}{}^2 \mu_{L_i} \dot{m}_L{}^2} \tag{B1}$$

This expression states that the mass rate of ablation less the mass rate of vaporization (i.e., the quantity of liquid flowing off the nose) is proportional to the liquid density, the square of the average thermal conductivity of the liquid, the square of the temperature at the gas-liquid interface, the shear gradient at the interface, and is inversely proportional to the liquid viscosity at the interface, the square of the heat capacity of the liquid and the square of the mass-rate of liquefaction. The coordinate system to which this and subsequent equations refer is stationary with respect to the gas-liquid interface as shown in the following sketch.

Shock

Gas-vapor boundary layer

s

Liquid layer

y

o

$\dot{m}_V$ $\dot{m}_L$

Body

Gas-liquid interface
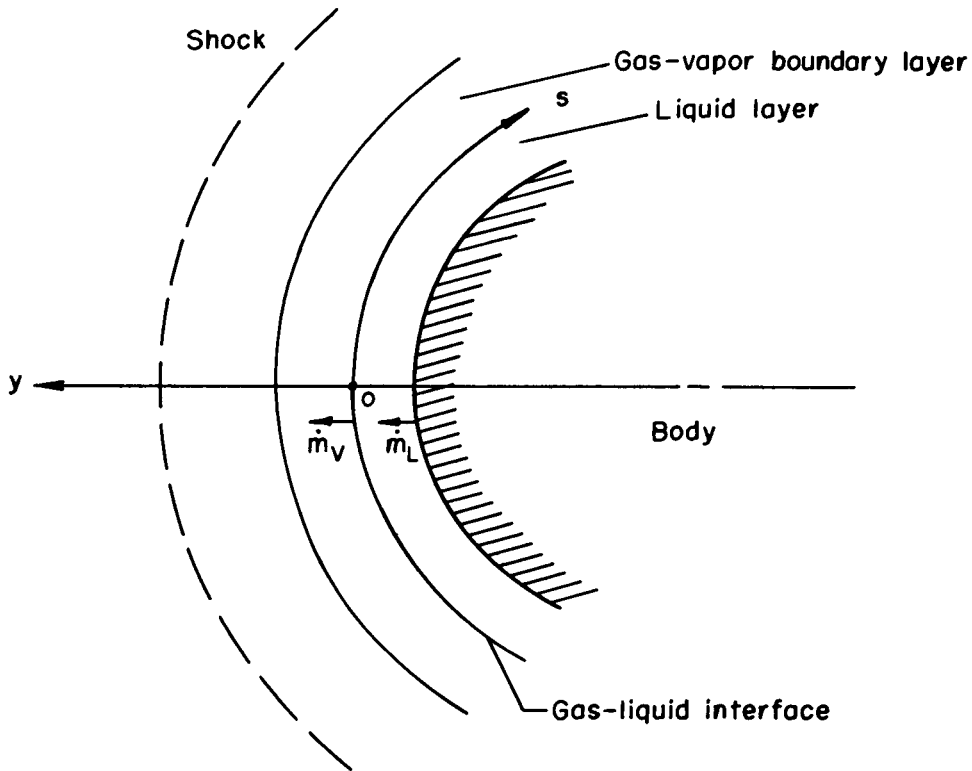
In the presence of vaporization, the aerodynamic heat-transfer rate at the interface must be balanced by the heat of vaporization in addition to the heat capacity of the solid and the liquid. Therefore, the energy balance equation may be written

$$\dot{q}_i = \dot{m}_L H_L + \dot{m}_V L_V \tag{B2}$$

where the heat capacity of the solid and liquid is

$$H_L = L_S + \bar{c}_S(T_m - T_S) + c_{p_L} \frac{T_i - T_m}{2} \tag{B3}$$

and L_S is the latent heat of fusion and L_V is the latent heat of vaporization.

The effect of mass injection into the boundary layer is to reduce the heat-transfer rate and shear at the interface. Therefore, we can write

$$\frac{\dot{q}_i}{\dot{q}_o} = \frac{\tau_i}{\tau_o} = \psi \tag{B4}$$

CONFIDENTIAL

where ψ is often referred to as the "blowing" parameter and has been the subject of numerous investigations (see, e.g., refs. 15 through 18). This parameter may be defined in terms of the driving enthalpy and mass injection rate as (see ref. 14)

$$\psi = 1 - aM^b(h_t - h_i) \frac{\dot{m}_V}{\dot{q}_o} \tag{B5}$$

where M is the ratio of the molecular weights of air to the injected vapor and a and b are empirically determined constants. The rate of mass injection may be related to the vapor pressure by (ref. 14)

$$\frac{p_t}{p_V} = 1 - aM^{b-1} + \frac{\dot{q}_o}{M(h_t - h_i)\dot{m}_V} \tag{B6}$$

At the stagnation point the shear gradient may be written (refs. 14 and 19)

$$\tau_o' = \frac{\dot{q}_o}{h_t - h_i} \frac{1}{r} \sqrt{2\frac{p_t}{\rho_t}} \, Pr_t^{2/3}$$

Substitution of this relation along with expression (B4) into equation (B1) yields

$$1 - \frac{\dot{m}_V}{\dot{m}_L} = \frac{2\rho_L \bar{k}_L^2 (T_i)^2 \sqrt{2(p_t/\rho_t)} \, Pr_t^{2/3}\psi\dot{q}_o}{(h_t - h_i)r\mu_{L_i}\dot{m}_L^3 c_{p_L}^2 A^2} \tag{B7}$$

The combination of equations (B2), (B4), and (B5) results in

$$\frac{\dot{q}_o}{\dot{m}_L} = H_L + \frac{\dot{m}_V}{\dot{m}_L} [L_V + aM^b(h_t - h_i)] \tag{B8}$$

for the energy balance equation. Therefore, consistent with the definition of the effective heat capacity employed in the text

$$Q^* = \frac{\dot{q}_o}{\dot{m}_L} = H_L + \frac{\dot{m}_V}{\dot{m}_L} [L_V + aM^b(h_t - h_i)] \tag{B9}$$

For materials whose viscosity and vapor pressure are steep functions of temperature we may write

$$\mu_L = \exp\!\left(\frac{A}{T} - B\right)$$

$$p_V = \exp\!\left(-\frac{C}{T} + D\right)$$

(B10)

where A, B, C, and D are constants. Then

$$\mu_L \sim p_V^{-A/C}$$

and (as suggested in ref. 14)

$$\mu_{L_i} = \mu_{L_t}\!\left(\frac{p_{V_i}}{p_t}\right)^{-A/C}$$

(B11)

where μ_{L_t} is the viscosity at the temperature at which the vapor pressure is equal to the stagnation pressure. In view of equations (B9) and (B11), expression (B7) finally may be written

$$1 - \frac{Q^* - H_L}{L_V + aM^b(h_t - h_i)} = \frac{2\rho_L \bar{k}_L^{\,2}(T_i)^2\sqrt{2(p_t/\rho_t)}\;\mathrm{Pr}_t^{\,2/3}Q^{*3}\psi}{r(h_t - h_i)\mu_{L_t}\dot{q}_o^{\,2}c_{p_L}^{\,2}A^2}\left(\frac{p_t}{p_{V_i}}\right)^{-A/C}$$

(B12)

where, by virtue of equations (B6) and (B9),

$$\frac{p_t}{p_{V_i}} = 1 + \frac{1}{M}\frac{Q^*}{Q^* - H_L}\left(\frac{L_V}{h_t - h_i} + \frac{aM^b H_L}{Q^*}\right)$$

(B13)

and, from expressions (B5) and (B9),

$$\psi = 1 - \frac{aM^b(h_t - h_i)(Q^* - H_L)}{Q^*[L_V + aM^b(h_t - h_i)]}$$

(B14)

Consider now equation (B12) in the following three limiting cases as it applies to test model and full-scale missile.

Case (a) Liquefaction with no vaporization ($\dot{m}_V = 0$):

Since $\dot{m}_V = 0$ for this case it follows from equations (B5) and (B9) that $\psi = 1$ and $Q^* = H_L$ and equation (B12) reduces to

$$1 = \frac{2\rho_L \bar{k}_L^{\,2}(T_i)^2\sqrt{2(p_t/\rho_t)}\;\mathrm{Pr}_t^{\,2/3}Q^{*3}}{r(h_t - h_i)\mu_{L_i}\dot{q}_o^{\,2}c_{p_L}^{\,2}A^2}$$

(B15)

Now the density of the liquid, the stagnation Prandtl number, and the ratio of stagnation pressure to stagnation density will be the same for model and missile. Furthermore, the thermal conductivity of the liquid can be considered approximately equal in both cases since it varies relatively slowly with temperature compared to the viscosity. If we note that (ref. 4)

$$\frac{(\dot{q}_o)_{mo}}{(\dot{q}_o)_{mi}} = \frac{D_{mi}}{D_{mo}}$$

and, for large flight velocities,

$$\frac{(h_t - h_i)_{mo}}{(h_t - h_i)_{mi}} \approx 1$$

then equation (B15) may be expressed in the form

$$\frac{Q^*_{mo}}{Q^*_{mi}} = \frac{(H_L)_{mo}}{(H_L)_{mi}} = \left[\frac{(\mu_{L_i})_{mo}}{(\mu_{L_i})_{mi}}\right]^{1/3}\left[\frac{(T_i)_{mi}}{(T_i)_{mo}}\right]^{2/3}\left(\frac{D_{mi}}{D_{mo}}\right)^{1/3}$$

It is evident from equations (B3) and (B10) that the above relation can be evaluated only for materials for which the thermal properties in its liquid state are known. For this reason, the variation of Q^*_{mo}/Q^*_{mi} with the scale factor D_{mi}/D_{mo} for two values of the interfacial temperature for the missile have been calculated for pyrex glass. The results are shown in figure 9. The thermal properties of pyrex employed in this calculation were obtained from references 7 and 14. Thus, a melting temperature of 3000° R was employed. In figure 9, the curve $T_i/T_m = 1.5$ corresponds to a flight altitude of 60,000 feet at a velocity of 17,000 feet per second according to the calculations of reference 7. Based on an extrapolation of these calculations, the curve $T_i/T_m = 2$ corresponds to a flight velocity in excess of 22,000 feet per second. Although the results shown in this figure are strictly applicable to pyrex glass, they should nevertheless hold qualitatively for materials which have a high liquid viscosity. From the standpoint of duplicating ablation by liquefaction of the surface material on a missile by means of a test model, the advantage of using large-scale facilities is evident from figure 9. The missiles simulated by the present tests are approximately 150 times the size of the test models. It is indicated from figure 9, therefore, that the largest probable factor for the ratio of model to missile effective heat capacities is approximately 1.1.

Case (b) Strong vaporization with high viscosity ($\dot{m}_V/\dot{m}_L \to 1$):

If there is strong vaporization on both model and missile, then

$$H_L \ll Q^*$$

and expressions (B13) and (B14) reduce to

$$\frac{p_t}{p_{V_i}} \approx 1 + \frac{L_V}{M(h_t - h_i)}$$

and

$$\psi \approx \frac{L_V}{L_V + aM^b(h_t - h_i)}$$

respectively. Since the driving enthalpy, $h_t - h_i$, is essentially dupli-
cated in model and missile, the above parameters will be approximately
the same in both cases.[4] If, in addition, the liquid viscosity is high,
then the right-hand member of equation (B12) will be very small and, in
the limit, this equation may be expressed in the form

$$\frac{Q^*_{mo}}{Q^*_{mi}} = \frac{[L_V + aM^b(h_t - h_i)]_{mo}}{[L_V + aM^b(h_t - h_i)]_{mi}}$$

Again the driving enthalpy is the important parameter. The result for
Q^* indicated by the above expression is similar to that obtained theo-
retically in reference 14 and verified experimentally (for teflon) in
reference 20. In this limiting case, therefore, $Q^*_{mo} \to Q^*_{mi}$.

Case (c) Strong vaporization with moderate viscosity ($\dot{m}_V/\dot{m}_L < 1$):

In this case, the term on the right in equation (B12) cannot be
neglected. If the fraction of liquid vaporized is the same in model and
missile, then

$$\left(\frac{\dot{m}_V}{\dot{m}_L}\right)_{mo} = \left(\frac{\dot{m}_V}{\dot{m}_L}\right)_{mi}$$

and the left-hand member of equation (B12) is the same for both model and
missile since from equation (B9)

---

[4]Since the assumption of Lewis number equal to unity is employed
(see refs. 7 and 14), it follows that the molecular weight ratio, M, is
equal in both model and missile.

$$\frac{Q^* - H_L}{L_V + aM^b(h_t - h_i)} = \frac{\dot{m}_V}{\dot{m}_L} \qquad (B16)$$

Equation (B12) then becomes (for strong vaporization)

$$\frac{Q^*_{mo}}{Q^*_{mi}} = \left[\frac{(\mu_{Lt})_{mo}}{(\mu_{Lt})_{mi}}\right]^{1/3}\left[\frac{(T_i)_{mi}}{(T_i)_{mo}}\right]^{2/3}\left(\frac{D_{mi}}{D_{mo}}\right)^{1/3}$$

which, it will be noted, is similar to the limiting expression obtained for no vaporization (case (a)). In the present case, however,

$$\frac{(\mu_{Lt})_{mo}}{(\mu_{Lt})_{mi}} = \left[\frac{(p_t)_{mo}}{(\rho_t)_{mi}}\right]^{-A/C} = \left(\frac{D_{mi}}{D_{mo}}\right)^{-A/C}$$

so that

$$\frac{Q^*_{mo}}{Q^*_{mi}} = \left[\frac{(T_i)_{mi}}{(T_i)_{mo}}\right]^{2/3}\left(\frac{D_{mi}}{D_{mo}}\right)^{1/3(1-A/C)}$$

Since $(T_i)_{mo}/(T_i)_{mi} > 1$, it is clear that there is some minimum value of A/C (< 1) for which $Q^*_{mo} = Q^*_{mi}$. For values of A/C greater than this minimum value, $Q^*_{mo} < Q^*_{mi}$ and the test model results will be conservative with respect to full-scale results. The term "conservative" is used in the sense that a greater percentage of material is lost on the model than would be lost on the simulated missile. In the case of pyrex glass, $A/C \approx 0.80$. For other materials for which $A/C \ll 1$, the test model results for Q^* in the present case will be greater by a factor always less than that which was observed for no vaporization (case (a)).

If

$$\left(\frac{\dot{m}_V}{\dot{m}_L}\right)_{mo} > \left(\frac{\dot{m}_V}{\dot{m}_L}\right)_{mi}$$

the left-hand member of equation (B12) will always be less in the case of the model. Therefore, the ratio Q^*_{mo}/Q^*_{mi} will be less than in the previous case just considered; namely $(\dot{m}_V/\dot{m}_L)_{mo} = (\dot{m}_V/\dot{m}_L)_{mi}$.

Finally, for the case where

$$\left(\frac{\dot{m}_V}{\dot{m}_L}\right)_{mo} < \left(\frac{\dot{m}_V}{\dot{m}_L}\right)_{mi}$$

equation (B16) expresses the fact that (noting that $H_L \ll Q^*$) $Q^*_{mo} < Q^*_{mi}$. Therefore the effective heat capacity determined from the tests will again be conservative with respect to the full-scale values.

On the basis of the foregoing analysis for the three limiting cases, $\dot{m}_V/\dot{m}_L = 0$, $\dot{m}_V/\dot{m}_L < 1$, and $\dot{m}_V/\dot{m}_L \to 1$, it is indicated that simulator test results are least applicable when no vaporization occurs. Thus, the results presented in figure 9 may be considered representative of an approximate maximum correction to simulator test results for Q^* in order to apply them to the full-scale missile.

REFERENCES

1. Roberts, Leonard: A Theoretical Study of Stagnation-Point Ablation. NACA TN 4392, 1958.

2. Rashis, Bernard, Witte, William G., and Hopko, Russell N.: Qualitative Measurements of the Effective Heats of Ablation of Several Materials in Supersonic Air Jets at Stagnation Temperatures Up to 11,000° F. NACA RM L58E22, 1958.

3. Neice, Stanford E., Carson, James A., and Cunningham, Bernard E.: Experimental Investigation of the Simulation of Atmospheric Entry of Ballistic Missiles. NACA RM A57I26, 1957.

4. Eggers, A. J., Jr.: A Method for Simulating the Atmospheric Entry of Long-Range Ballistic Missiles. NACA RM A55I15, 1955.

5. Eggers, Alfred J., Jr., Allen, H. Julian, and Neice, Stanford E.: A Comparative Analysis of the Performance of Long-Range Hypervelocity Vehicles. NACA TN 4046, 1957. (Supersedes NACA RM A54L10)

6. Allen, H. Julian, and Eggers, A. J., Jr.: A Study of the Motion and Aerodynamic Heating of Missiles Entering the Earth's Atmosphere at High Supersonic Speeds. NACA TN 4047, 1957. (Supersedes NACA RM A53D28)

7. Lees, Lester: Similarity Parameters for Surface Melting of a Blunt Nosed Body in a High Velocity Gas Stream. ARS Journal, vol. 29, no. 5, May 1959, pp. 345-354.

8. Lees, L.: Laminar Heat Transfer Over Blunt-Nosed Bodies at Hypersonic Flight Speeds. Jet Propulsion, vol. 26, no. 4, Apr. 1956, pp. 259-269

9. Eggers, A. J., Jr., Hansen, C. Frederick, and Cunningham, Bernard E.: Stagnation-Point Heat Transfer to Blunt Shapes in Hypersonic Flight, Including Effects of Yaw. NACA TN 4229, 1958.

10. Straus, Sidney, and Wall, Leo A.: Pyrolysis of Polyamides. Journal of Research of the National Bureau of Standards, vol. 60, no. 1, Jan. 1958, pp. 39-45.

11. Hartwig, F. W.: Development and Application of a Technique for Steady State Aerodynamic Heat Transfer Measurements. GALCIT Hypersonic Research Proj., Memo. 37, June 1957.

12. Churchill, Ruel V.: Modern Operational Mathematics in Engineering. McGraw-Hill Book Co., 1944, pp. 106-109 and 214-215.

13. Brogan, Thomas R.: Electric Arc Gas Heaters for Re-entry Simulation and Space Propulsion. Res. Rep. 35, AVCO Res. Lab., Sept. 1958.

14. Bethe, Hans A., and Adams, Mac C.: A Theory for the Ablation of Glassy Materials. Res. Rep. 38, AVCO Res. Lab., Nov. 1958.

15. Baron, Judson R.: The Binary-Mixture Boundary Layer Associated With Mass Transfer Cooling at High Speeds. Massachusetts Institute of Technology, Naval Supersonic Laboratory, Tech. Rep. 160, May 1956.

16. Reshotko, E., and Cohen, C. B.: Heat Transfer at the Forward Stagnation Point of Blunt Bodies. NACA TN 3513, 1955.

17. Rubesin, M. W., Pappas, C. C., and Okuno, A. F.: The Effect of Fluid Injection on the Compressible Turbulent Boundary Layer - Preliminary Tests on Transpiration Cooling of a Flat Plate at $M = 2.7$ With Air as the Injected Gas. NACA RM A55I19, 1955.

18. Rubesin, M. W.: The Influence of Surface Injection on Heat Transfer and Skin Friction Associated With the High-Speed Turbulent Boundary Layer. NACA RM A55L13, 1956.

19. Fay, J. A., Riddell, F. R., and Kemp, N. H.: Stagnation Point Heat Transfer in Dissociated Air Flow. Jet Propulsion, vol. 27, no. 6, June 1957, pp. 672-674.

20. Georgiev, Steven, Hidalgo, Henry, and Adams, Mac C.: On Ablation for the Recovery of Satellites. Res. Rep. 47, AVCO Res. Lab., March 1959.
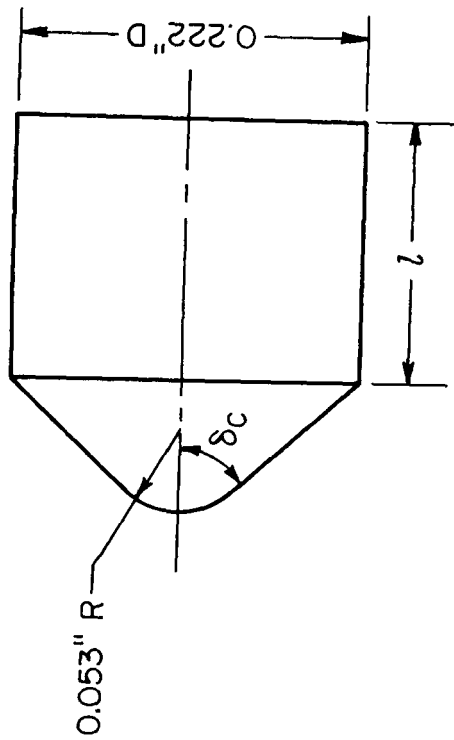
δ_c, deg	l, in.
40	0.077
50	.110
60	.118
70	.127
90	.139

Material: Polypenco nylon

Figure 1.- Dimensions of test models.
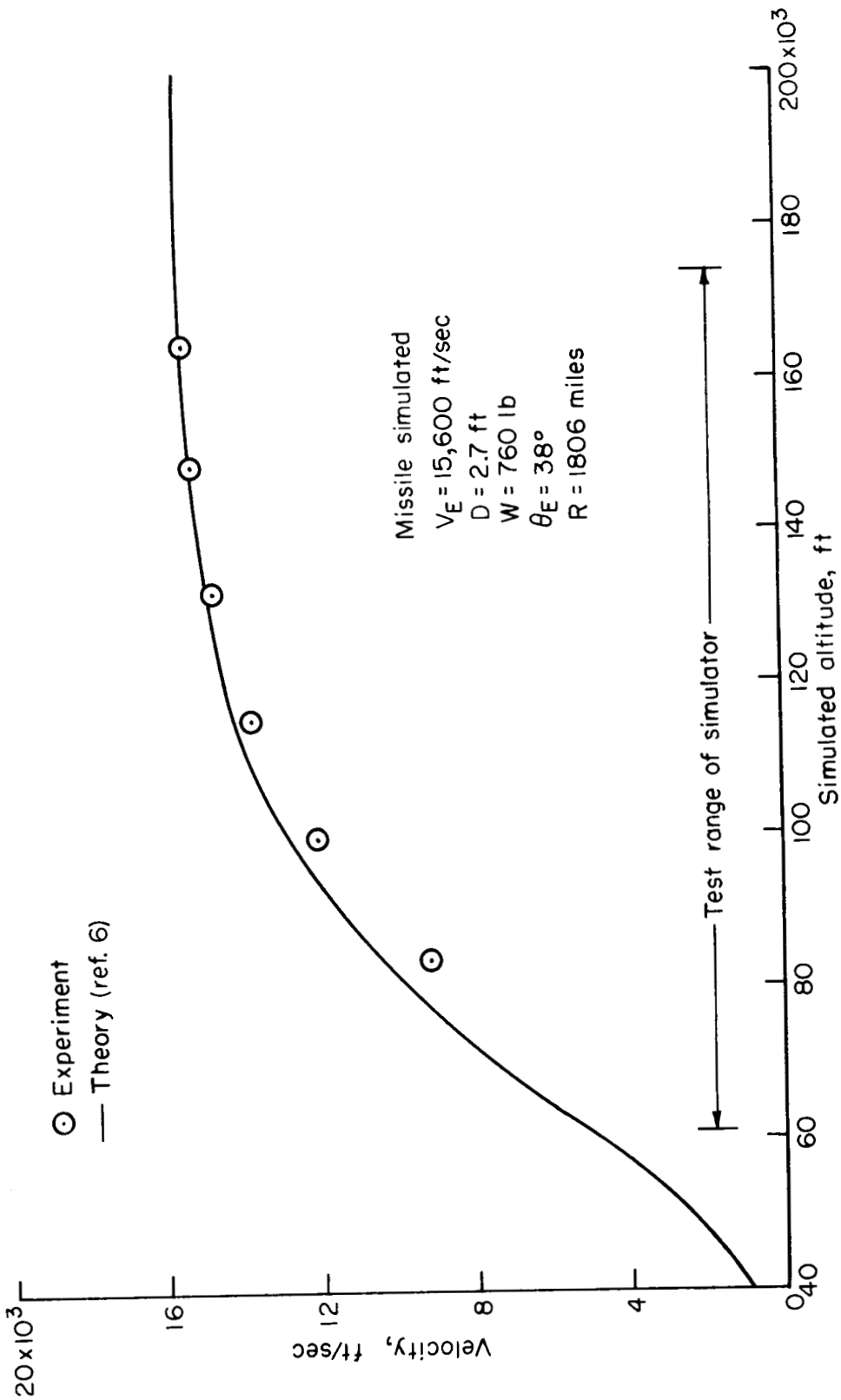
Figure 2.- Comparison of theoretical variation of velocity with altitude for full-scale missile with experimental variation obtained with test model.
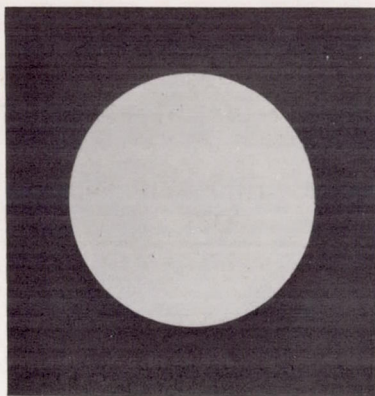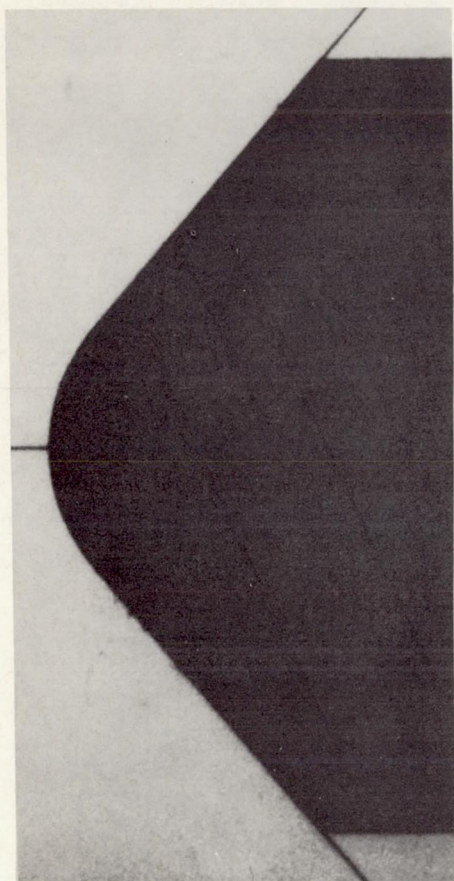
Before test

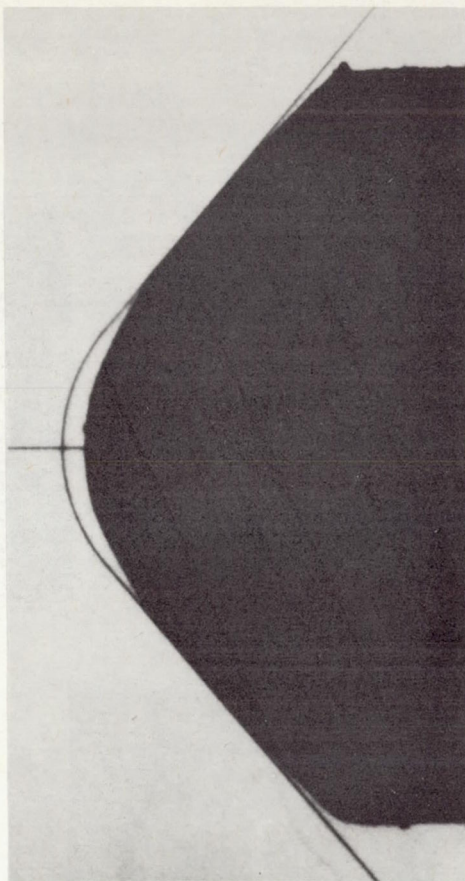V_E = 13,300 ft/sec
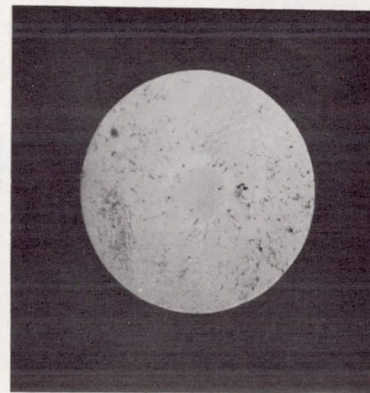
A-24631-15

V_E = 19,800 ft/sec

After test

Figure 3.- Typical preflight and postflight models; $\delta_c = 50^\circ$.

Unfired model V_E = 13,300 ft/sec V_E = 19,800 ft/sec
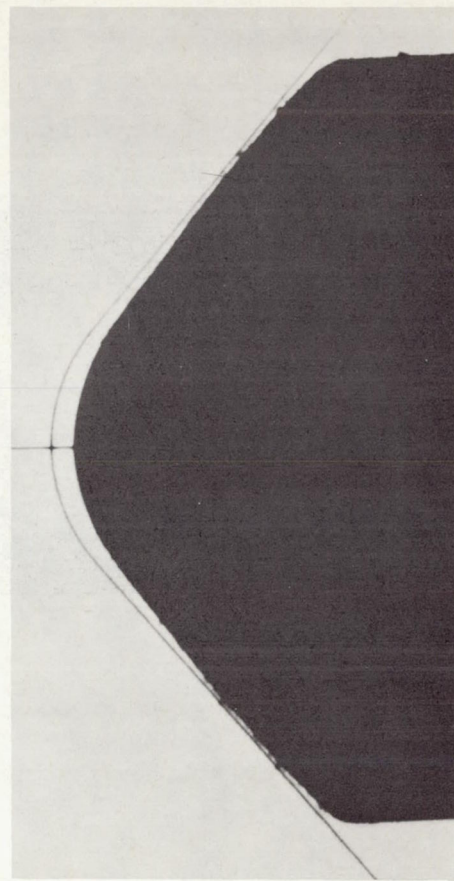
Figure 4.- Comparison of preflight and postflight model profiles; δ_c = 50°.
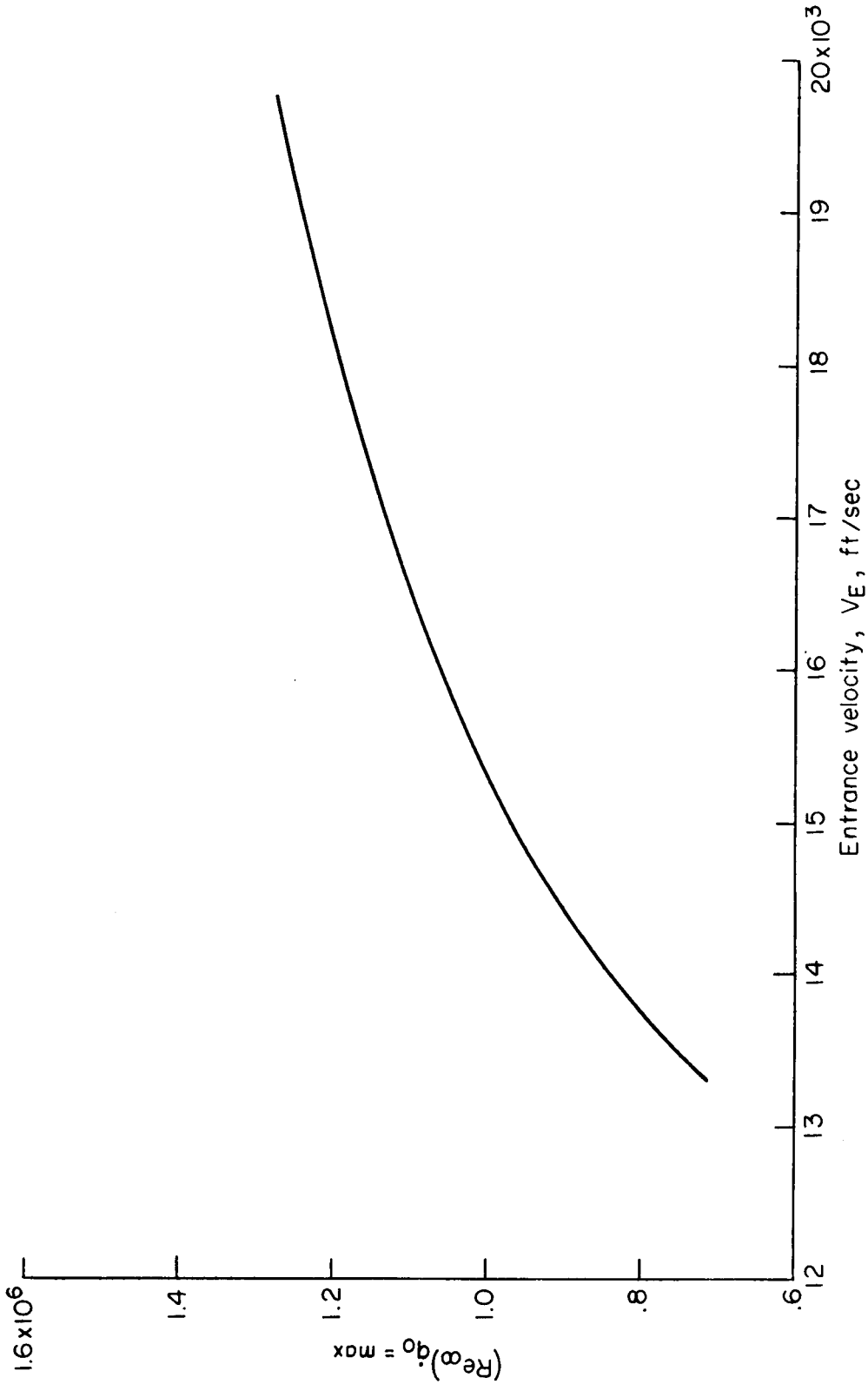
Figure 5.- Variation with entrance velocity of free-stream Reynolds number at point in trajectory corresponding to the maximum heat-transfer rate.

CONFIDENTIAL
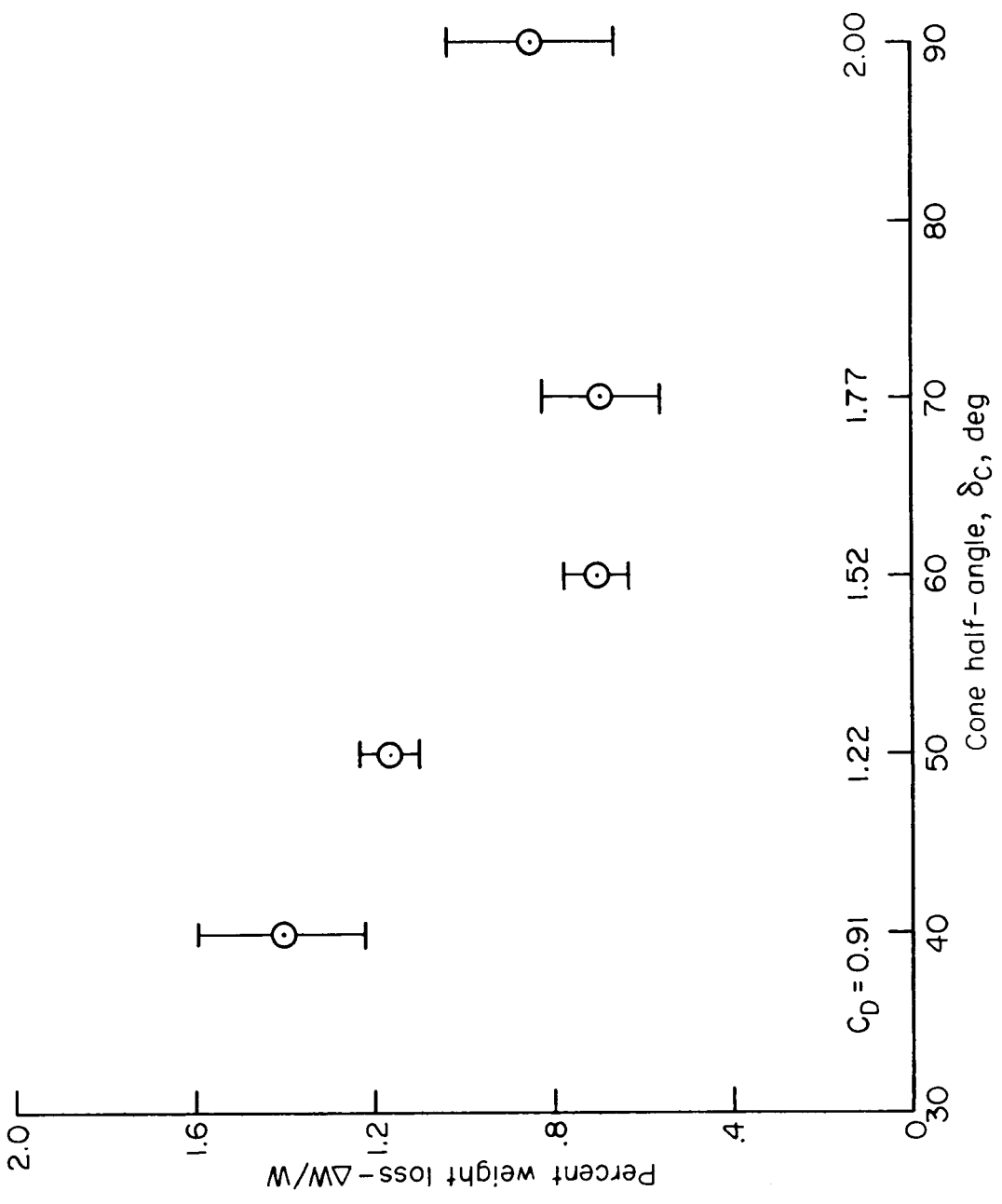
Figure 6.- Variation of ablation weight loss with nose shape; V_E = 15,600 feet per second.
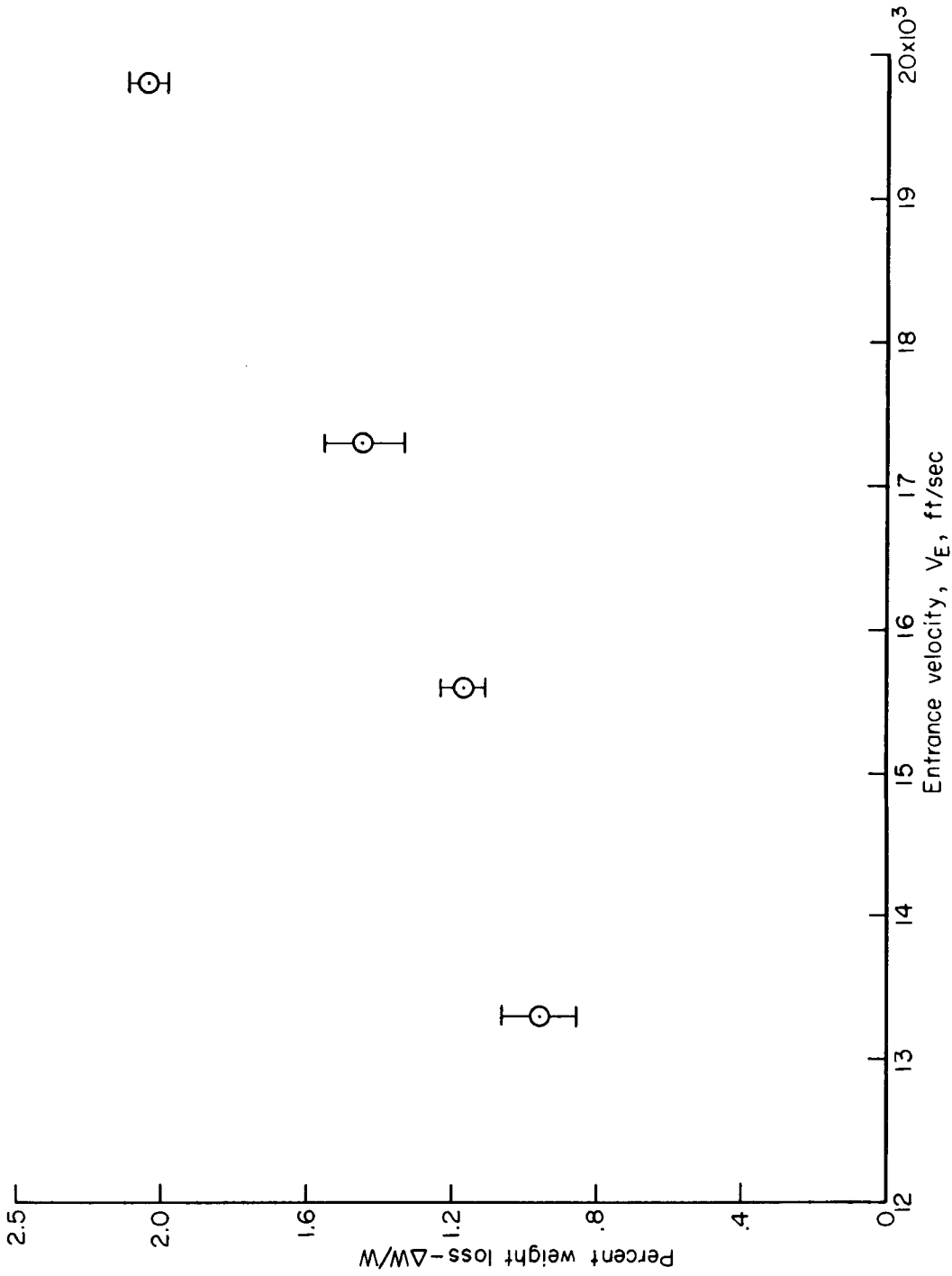
Figure 7.- Variation of ablation weight loss with entrance velocity; $\delta_c = 50°$.
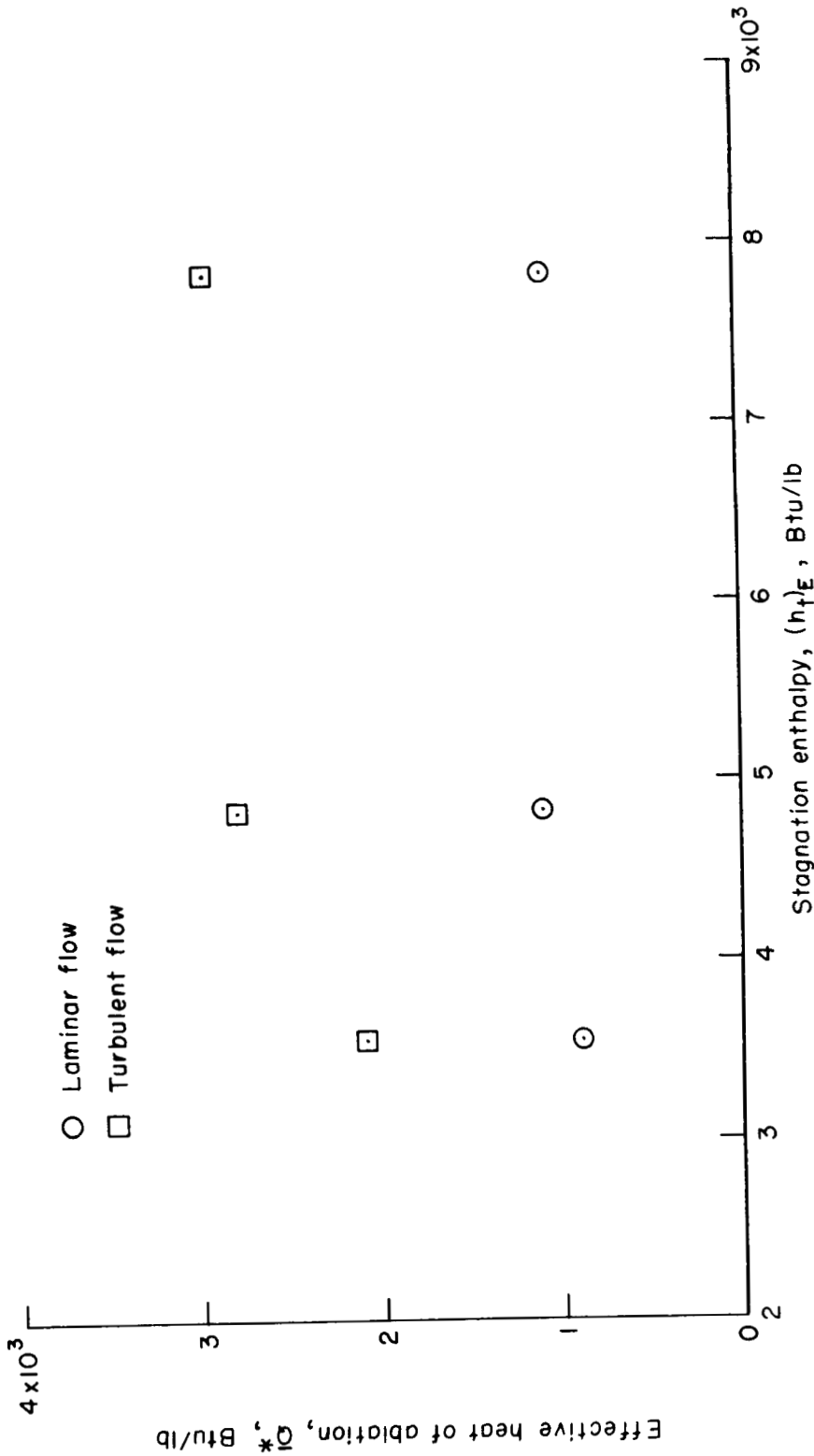
Figure 8.– Variation of average effective heat of ablation with stagnation enthalpy corresponding to entry velocity.

No. 7740 Corning glass properties (refs. 7 and 14)

$$L_s + \bar{c}_s(T_m - T_s) = 750 \text{ Btu/lb}$$

$$\mu_L = 0.0672 \exp\left[\frac{68{,}940}{T, °R} - 17\right] \text{ lb/ft-sec}$$

$$c_{P_L} = 0.33 \text{ Btu/lb-°F}; \quad T_m = 3000° \text{ R}$$

$(T_i/T_m)_{mi} = 2.0$
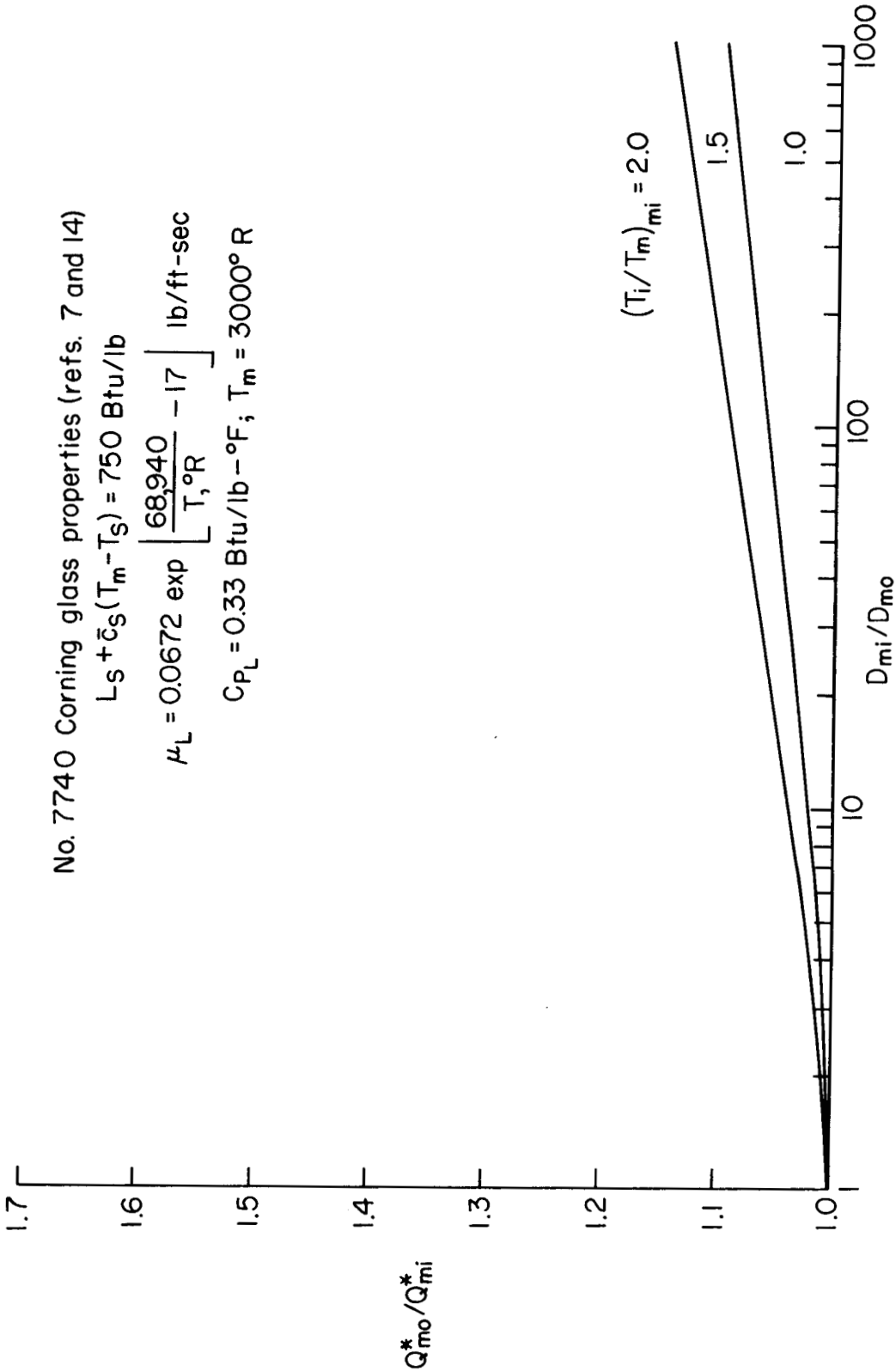
1.5

1.0

D_{mi}/D_{mo}

Q^*_{mo}/Q^*_{mi}

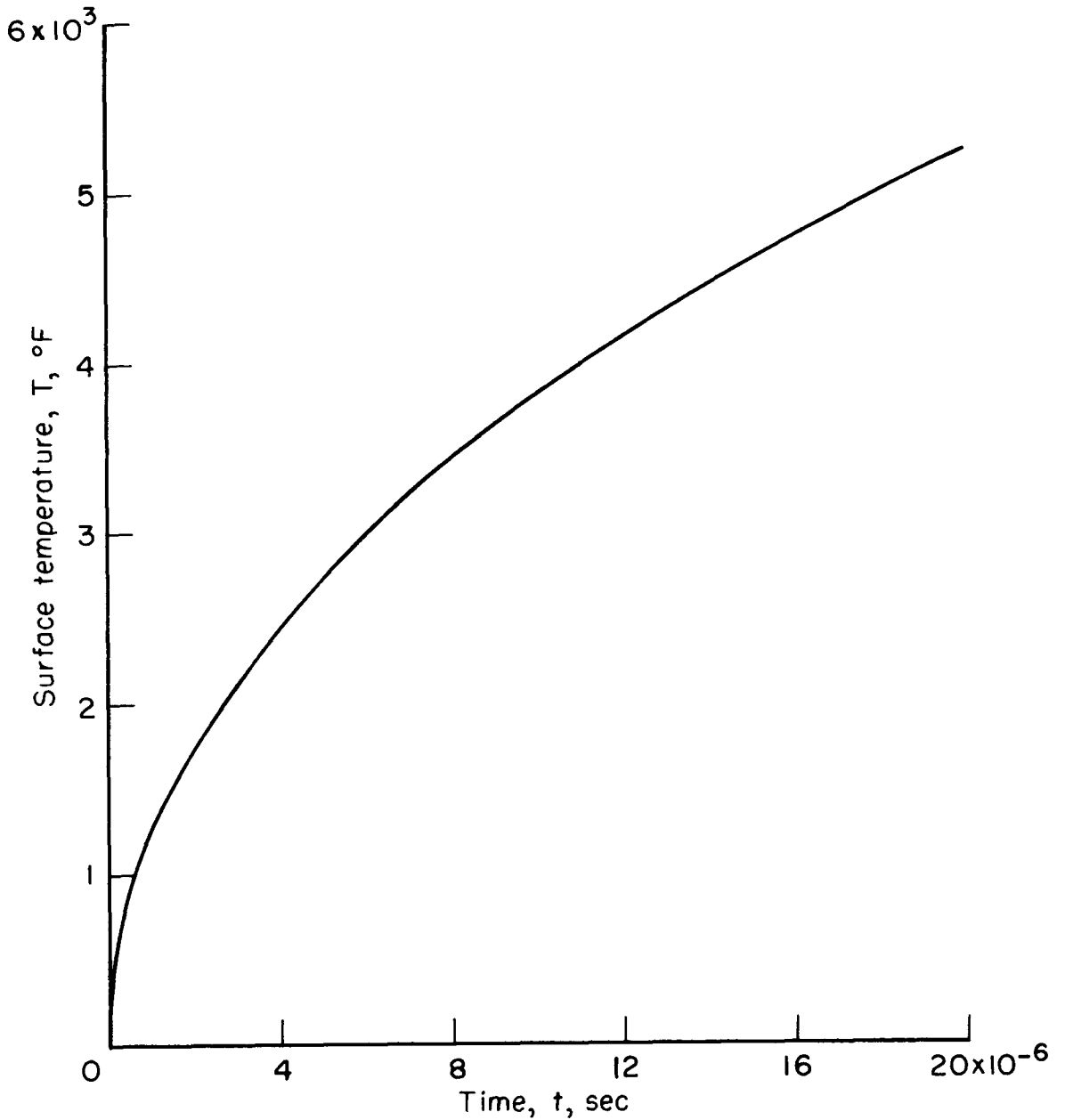Figure 9.- Effect of interfacial temperature and model scale on effective heat of ablation (no vaporization).

Figure 10.- Initial surface-temperature rise at the stagnation point of a
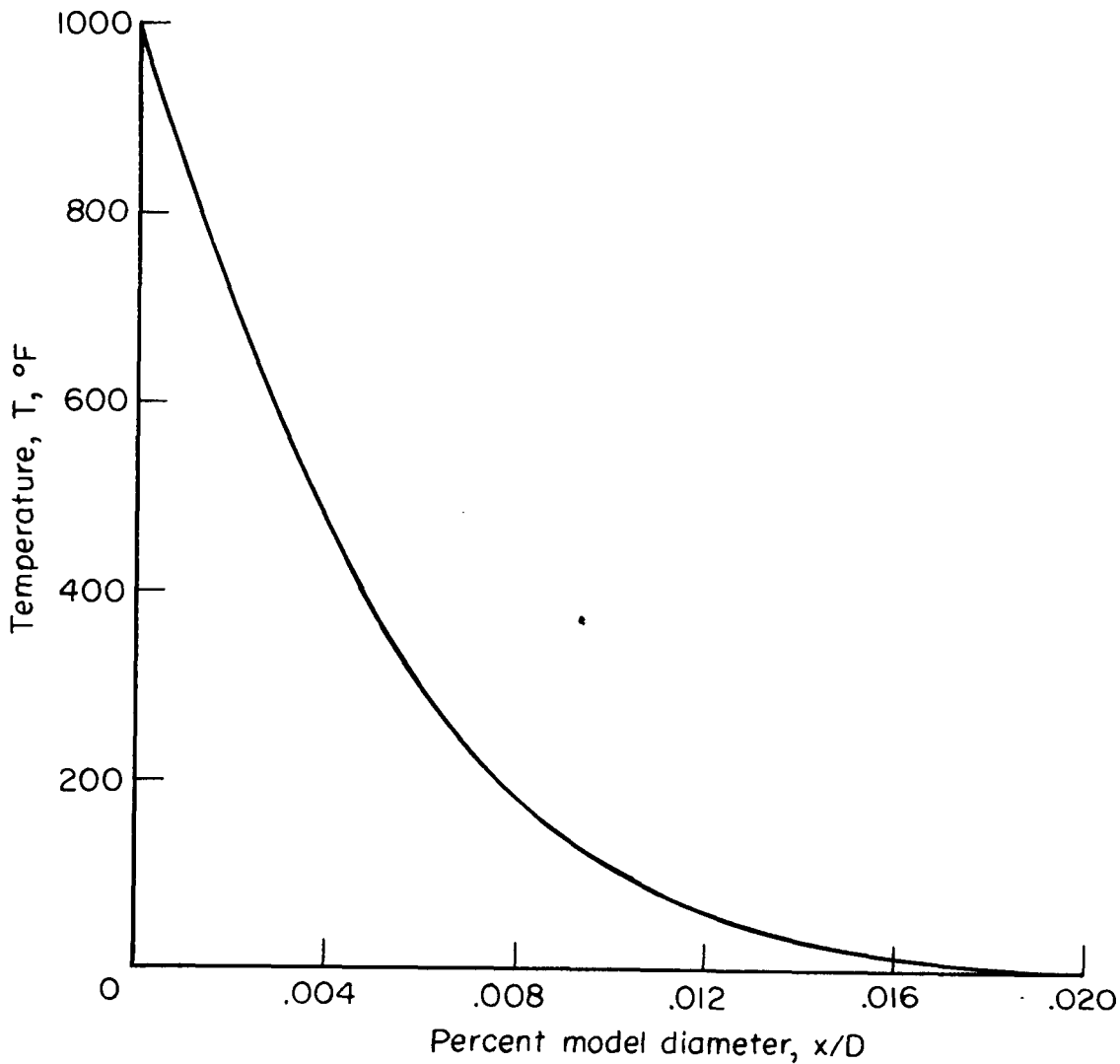nylon model during flight in the simulator; V_E = 15,600 feet per second.

Figure 11.- Temperature distribution in nylon model at beginning of flight through simulator; V_E = 15,600 feet per second.